Rotational Stiffness of Wood Truss Joints in Lateral and Diagonal Bracing and Truss–Wall Connections

Milad Mohamadzadeh, A.M.ASCE[1]; Daniel P. Hindman, M.ASCE[2]; and Annaliese G. Whaley[3]

Abstract: The modeling and structural analysis of roof systems composed of metal plate–connected wood trusses (MPCWTs) require a detailed understanding of the rotational stiffness associated with various connections of the MPCWTs to the bracing elements and to the walls supporting the roof. The purpose of this study was to measure the rotational stiffness of several truss–bracing and truss–wall connections attached to MPCWTs to be used for structural modeling. Bracing included discrete and continuous bracing supporting the top and bottom chords of trusses. Truss–wall connections used single fasteners and proprietary sheet-metal connections. For the bracing connections, the rotational stiffness of the discrete bracing was greater than the rotational stiffness of the continuous bracing. Joist hanger–style truss–wall connections had greater rotational stiffness compared with hurricane ties or single-fastener connections. The rotational stiffness of hurricane ties was much greater when the applied torque caused a tension force in the hurricane tie versus a compression force. The rotational stiffness of hurricane ties from two different manufacturers was not significantly different. **DOI: 10.1061/(ASCE)AE.1943-5568.0000349.** © *2019 American Society of Civil Engineers.*

Author keywords: Rotational stiffness; Metal plate–connected wood trusses; Metal connectors; Nailed connections.

Introduction

Behavior of Structural Connections

The behavior of mechanical joints in timber structures has been a frequent topic of research. Mechanical joints are often idealized as rigid or hinged, whereas the actual behavior of joints is usually characterized as semirigid (Kanerva et al. 2004). Semirigid behavior has been modeled using either linear elastic or nonlinear models to evaluate the behavior of the structure. For models used for the moment–rotation behavior of joints, linear elastic theory is applicable up to service-limit states for the majority of structures. However, linear elastic theory is not as accurate as nonlinear models in predicting ultimate loads because local stress peaks can be overestimated due to material yielding (Kanerva et al. 2004).

Zaharia and Dubina (2006) studied the stiffness of bolted cold-formed steel truss joints in the design load ranges. Joint stiffness in design was considered because of changes in the American Iron and Steel Institute (AISI) standards for cold-formed steel truss design (AISI 2001). Previously, truss joints were assumed as pinned connections. Three experimental steps were followed, (1) tests on T-joint specimens, (2) tests on single lap joints, and (3) tests on the truss structure, in addition to computational models for rotational stiffness of truss joints (Zaharia and Dubina 2006). The rotational stiffness of truss joints tested in Steps 1 and 2 used a computational formula for model incorporation. Good agreement between experimental and computational models was found. The behavior of a single truss was found to be influenced not only by rotational stiffness but also by the axial stiffness of joints in the web member directions, although axial effects were smaller than rotational ones (Zaharia and Dubina 2006). This procedure of measuring joint stiffness experimentally, then applying the stiffness in modeling efforts can be applied to structures with metal plate–connected wood trusses (MPCWTs) as well.

Truss Joints

Connections in MPCWTs are the locations that transfer axial forces between elements and ensure the integrity of the truss assembly (Kassimali 2010). Gupta et al. (1992) investigated MPCWTs with semirigid joints using matrix structural analysis methods. Modifications were applied to derive element stiffness matrices and fixed end forces of members with one or both ends acting as semirigid connections. Three different joint assumptions were analyzed: pin, rigid, and semirigid joints. These joint assumptions had a notable influence on the amount of deflection. Joints with semirigid behavior deflected 34% less than pinned joints, and semirigid joints had 13% less moment capacity compared with rigid joints. Predictions of truss behavior and member forces were more accurate when semirigid joint behavior was considered (Gupta et al. 1992).

Šilih et al. (2005) studied the optimization of metal plate–connected plane timber trusses, with a special emphasis on joint flexibility. Nonlinear programming methods were used to optimize truss models. Such variables as truss configuration, span/depth ratio, number and type of diagonal and vertical members, and type of joint connections were taken into account in a single mathematical model. In the optimized model, joint flexibility increased maximum deflection by 10–15% for the timber truss (Šilih et al. 2005).

In a similar study, the shape and discrete sizing optimization of timber trusses considering flexibility were investigated (Šilih et al. 2010). Mixed-integer nonlinear programming (MINLP) was used as an optimization approach, and internal forces and deflections were calculated using finite-element analysis. Joint flexibility had a

[1]Structural Engineer, SKA&MD Structural Engineers, 12435 Park Potomac Ave., Suite 300, Potomac, MD 20854.

[2]Associate Professor, Virginia Tech, 1650 Research Center Dr., Blacksburg, VA 24061 (corresponding author). Email: dhidman@vt.edu

[3]Structural Engineer, BMC—Building Materials and Construction Solutions, 10589 Redoubt Road, Manassas, VA 20110.

Note. This manuscript was submitted on May 5, 2017; approved on October 10, 2018; published online on January 10, 2019. Discussion period open until June 10, 2019; separate discussions must be submitted for individual papers. This paper is part of the ***Journal of Architectural Engineering***, © ASCE, ISSN 1076-0431.

significant effect on the results of the analysis. Deflections due to slipping of the truss connections represented over 40% of the total deflections (Šilih et al. 2010). Therefore, accurate representation of the joint-stiffness performance is essential to accurately predict the deformation of MPCWTs.

Lateral Loading of Trusses

A recent topic of research on MPCWT roof systems involved the lateral loading of trusses by forces applied normal to the plane of the trusses. This loading condition has implications for wind loads and construction loads related to fall-arrest equipment. DeRenzis et al. (2012) investigated the effect of lateral and uplift loading applied to the performance of high-heel (energy-heel) styles of trusses compared with conventional low-heel trusses. Although the performance of high-heel trusses was less than that of conventional trusses, the use of oriented strandboard (OSB) sheathing rather than purlin systems for bracing was recommended to improve the strength and stiffness of the roof system. During testing, buckling and rotation of the hurricane clips attaching the trusses to the wall were observed (DeRenzis et al. 2012).

Several truss assemblies were tested for lateral loading of trusses caused by the activation of a fall-arrest system applying a horizontal load component to the truss. Koch et al. (2016) tested single mono-slope queen-post MPCWTs, whereas Morris and Hindman (2017) studied a 3.96-m-wide roof system composed of five trusses with various bracing configurations. In both studies, rotation of the hurricane clips attaching the trusses to the wall was observed, similar to observations by DeRenzis et al. (2012).

In the testing of truss assemblies to failure, Morris and Hindman (2017) also observed the rotation of various lateral bracing elements attached to the top chord of the truss. Fig. 1 is a schematic of the truss assembly tested, with locations of both lateral and diagonal bracing shown. Lateral bracing used included discrete bracing placed between the trusses, continuous bracing placed over the trusses, and engineered steel braces. Diagonal bracing and continuous bracing over the trusses are sometimes used as temporary bracing that is then removed before sheathing is applied.

The deformation of the truss assembly is presented in Fig. 2, with rotation of the trusses at the hurricane clips, bending of the truss elements, and rotation of the various lateral and diagonal bracing elements. An interesting behavior of the lateral bracing elements was a pinching behavior, in which a prying action on some fasteners caused withdrawal, whereas the truss members firmly held the other corner.

Rotation of the truss–wall connections and rotation of the truss-bracing elements were considered important contributions to the strength and stiffness of the overall truss assembly tested by Morris and Hindman (2017). The truss–wall connections were previously noted as contributors to the collapse of MPCWTs tested by DeRenzis et al. (2012) and Koch et al. (2016). To analyze structures in service-limit states, linear elastic theory can provide a good estimation of structural behavior (Kanerva et al. 2004) because Šilih et al. (2010) demonstrated that joint stiffness had a significant effect on the results of the structural analysis. The goal of this study was to measure the rotational stiffness of discrete and continuous bracing and truss–wall connections to provide data for modeling of MPCWT assemblies considering the semirigid behavior of joints. Only nailed connections were considered for the discrete and continuous bracing, whereas several different proprietary truss–wall connections were tested.

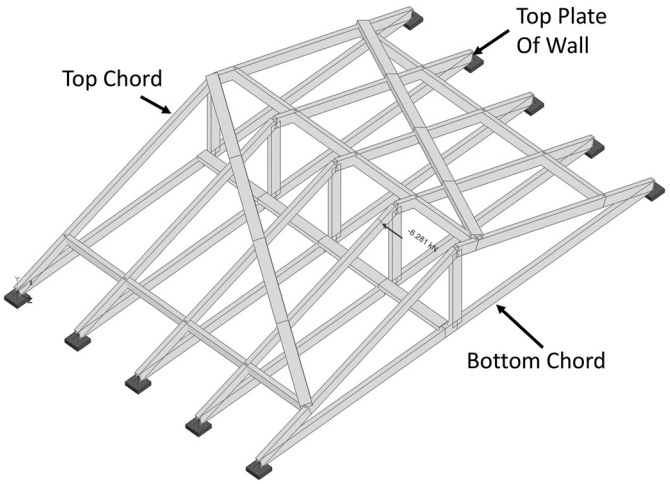

Fig. 1. Schematic of truss assembly tested by Morris and Hindman (2017) showing discrete bracing.

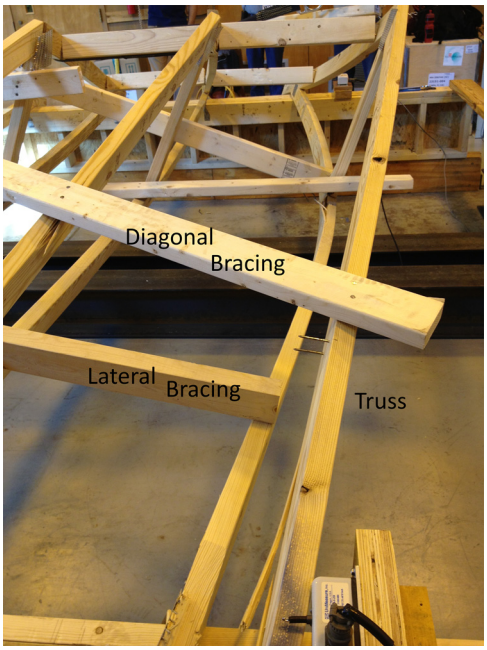

Fig. 2. Truss assembly from Morris and Hindman (2017) during testing.

Materials and Methods

Definition of Rotational Stiffness

Stiffness is defined as the rigidity of an object or the resistance against deformation under an applied force (Kanerva et al. 2004). Rotational stiffness depends on the angular rotation of the member as a function of an applied torque. Joints in structures may be subject to rotational stiffness depending on structural function. Eq. (1) was used to measure the rotational stiffness, k, of a joint. The equation assumes that linear elastic theory is applicable for the majority of structures in service-limit states (Kanerva et al. 2004).

$$k = \frac{M}{\theta} = \frac{PL}{\theta} \tag{1}$$

where M = moment at the joint; θ = rotation angle of the joint; and P = applied load at a moment arm of length L. The use of a

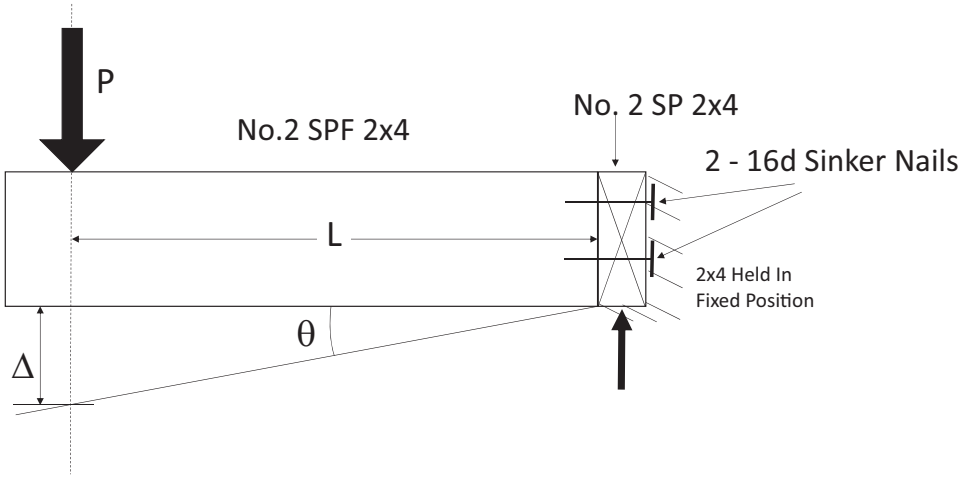

Fig. 3. Rotational stiffness test of the discrete bracing.

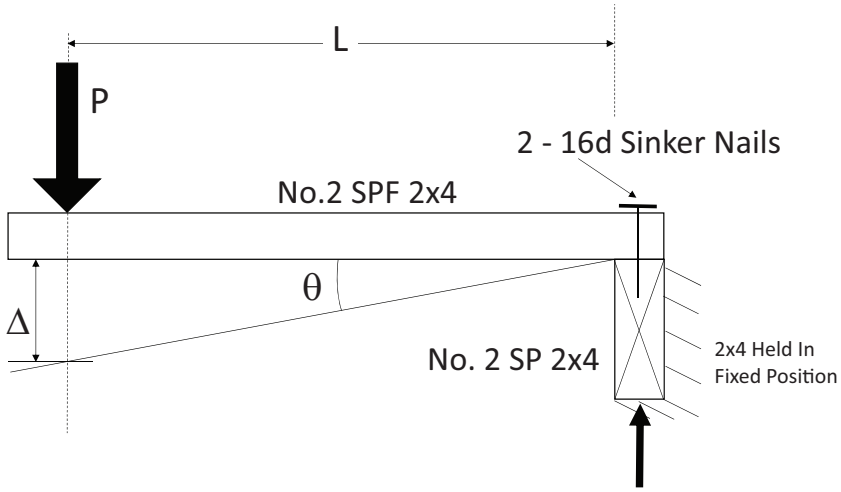

Fig. 4. Rotational stiffness test of the continuous bracing.

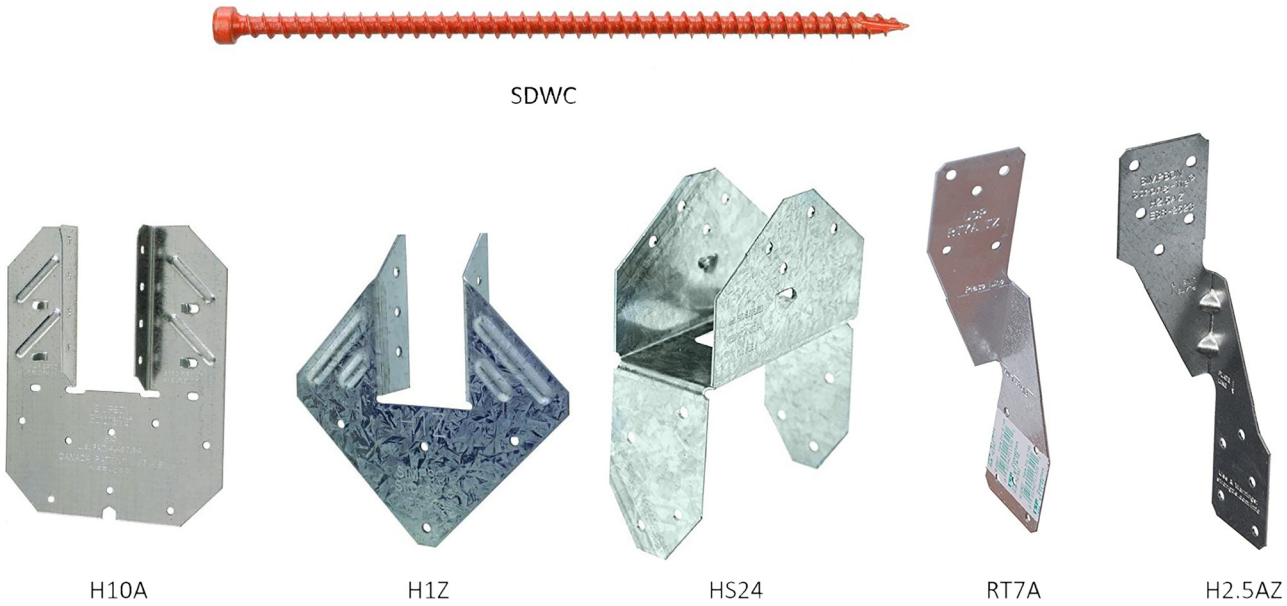

Fig. 5. Proprietary truss-to-wall connections tested in this study.

Table 1. Test specimens for truss-to-wall connections

Test	Manufacturer	Description	Number tested
RT7A-T	USP (MiTek)	Hurricane tie, load applied in tension	10
RT7A-C	USP (MiTek)	Hurricane tie, load applied in compression	10
RT7A-2	USP (MiTek)	Hurricane tie, placed on both sides of truss chord	8
H1Z	Simpson Strong-Tie	Diamond-shaped plate, attaches to face of top plate	8
H10A	Simpson Strong-Tie	Rectangular-shaped plate, attaches to face of top plate	8
HS24	Simpson Strong-Tie	Saddle-shaped connection, attaches to sides of truss and top plate	8
H2.5AZ-T	Simpson Strong-Tie	Hurricane tie, load applied in tension	8
H2.5AZ-2	Simpson Strong-Tie	Hurricane tie, placed on both sides of truss chord	8
SDWC	Simpson Strong-Tie	Strong-Drive SDWC truss screw	8
Control	N/A	Single 10d toenail	8

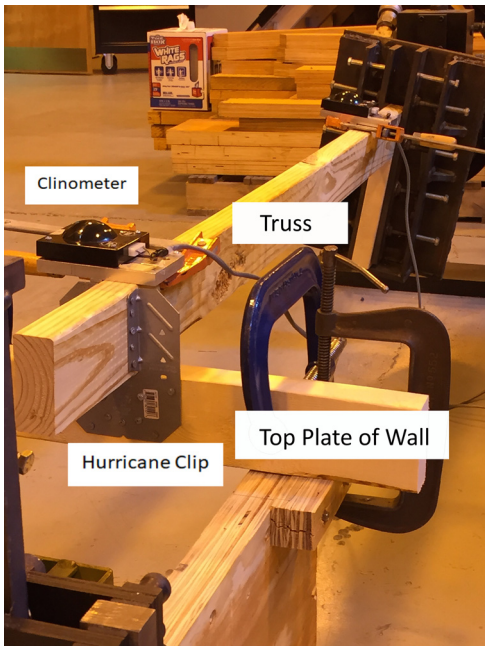

Fig. 6. Rotational stiffness measurement of the truss-to-wall connections.

cantilever beam arrangement to measure rotational stiffness was adopted for this testing. Calculations of the bending and shear deformation associated with the lumber sections were checked to ensure that these deformations remained negligible compared with the rotation of the cantilever arm.

Rotational Stiffness Measurement of Discrete Bracing

Discrete bracing elements, labeled *in-between* bracing by Morris and Hindman (2017), are composed of separate bracing elements placed between truss chords. The end grain of the bracing contacts the truss chord face, and the top surface is flush with the top of the trusses. The truss chord was represented by a section of No. 2 southern pine (SP) 2 × 4 (38.1 by 88.9 mm) clamped to a fixed bracket. The bracing element, or moment arm, was a No. 2 spruce–pine–fir (SPF) 2 × 4. Two 16d sinker nails (0.41 cm diameter, 8.89 cm long) were driven through the truss chord side grain and into the end grain of the bracing.

Force was applied at 0.508 m (20 in.) from the truss chord (Fig. 3) by an MTS Systems Corporation (Eden Prairie, Minnesota) universal testing machine with a maximum load capacity of 22.2 kN (5,000 lb) and a sensitivity of less than 1%. The displacement rate of the load was 12.5 mm/min (0.5 in./min). The deflection of the brace was measured directly under the point of loading with a potentiometer [254-mm (1.0-in.) range, sensitivity of 0.025 mm (0.001 in.)]. The brace was assumed to rotate about the bottom edge of the truss chord without crushing. Testing was concluded when the deflection reached 152 mm (6.0 in.). The horizontal displacement of the truss chord was monitored to ensure no movement occurred.

In total, 20 samples were tested to obtain the rotational stiffness of the discrete bracing joints. The moment was calculated as the load multiplied by the moment arm. The rotation angle θ was calculated using the triangular geometric relations of the displacement at the point of loading. The moment–rotation slope (M/θ) was used to calculate rotational stiffness, k, from Eq. (1).

Table 2. Rotational stiffness of discrete and continuous bracing

Bracing	Rotational stiffness k [N·m/degree (COV)]
Discrete	89.5 (29.1%)
Continuous	21.4 (49.7%)

Rotational Stiffness Measurement of Continuous Bracing

Continuous bracing elements are composed of a single section of lumber placed over the truss chords as a temporary brace during construction. The side grain of the bracing is connected to the side grain of the truss top chord. The truss chord was represented by a section of No. 2 SP 2 × 4 (38.1 by 88.9 mm) clamped to a fixed bracket. The bracing element, or moment arm, was a No. 2 SPF 2 × 4. Connections to the bracing used two 16d sinker nails [4.09-mm (0.161-in.) diameter, 107 cm (3.5 in.) long] nailed through the brace and into the truss top chord.

Force was applied 0.508 m (20 in.) from the truss chord (Fig. 4) by an MTS universal testing machine with a maximum load capacity of 22.2 kN (5,000 lb.) and a sensitivity of less than 1%. The displacement rate of the load was 12.5 mm/min (0.5 in./min). The deflection of the brace was measured directly under the point of loading with a potentiometer [254-mm (1.0-in.) range, sensitivity of 0.025 mm (0.001 in.)]. The brace was assumed to rotate about the leading edge of the truss chord with no crushing. Testing was concluded when the deflection reached 152 mm. The horizontal displacement of the truss chord was monitored to ensure no movement occurred.

In total, 20 samples were tested to obtain the rotational stiffness of the discrete bracing joints. The moment was calculated as the load multiplied by the moment arm. The rotation angle θ was calculated using the triangular geometric relations of the displacement at

loading. The moment–rotation slope (M/θ) was used to calculate rotational stiffness, k, from Eq. (1).

Rotational Stiffness Measurement of Truss–Wall Connections

The truss–wall connections serve to provide uplift resistance to the roof system, but they also resist rotation of the trusses imposed by a horizontal load. With the application of a horizontal load applied above the height of the truss–wall connection, the truss–wall connection experiences a torsion force about the axis of the truss bottom chord, as presented in Fig. 2. The testing of truss–wall connections used a cantilever beam test for rotational stiffness, with a centric moment applied to create rotation. The bottom chord was represented by a No. 2 2 × 4 SP lumber, 1.83 m (6 ft) long, and was attached to a perpendicular section of No. 2 2 × 4 SPF firmly attached to the test frame, representing the top plate of the wall. For ease of attachment, the stud representing the top plate of the wall was oriented edgewise for the face-applied truss–wall connections.

The truss–wall connections can be separated into three different groups: single-fastener connections, joist hanger–style connections, and hurricane ties. Fig. 5 presents the various proprietary truss–wall connections used. Single-fastener connections consisted of a single 10d common (0.12 in. in diameter, 2.875 in. long) toenail, driven at a 30-degree angle to vertical (AWC 2015), and a Strong-Drive (Simpson Strong-Tie, Pleasanton, California) SDWC truss screw. The 10d toenail connection was considered the control for this experiment. The SDWC was applied from the underside of the top plate of the wall and drilled into the bottom of the truss top chord.

Joist hanger–style connections were proprietary folded sheet-metal connections containing a pocket or saddle to support the truss bottom chord. These connections included the H1Z, with a diamond-shaped plate mounted to the wall top plate; the H10A, with a large rectangular plate mounted to the wall top plate; and the

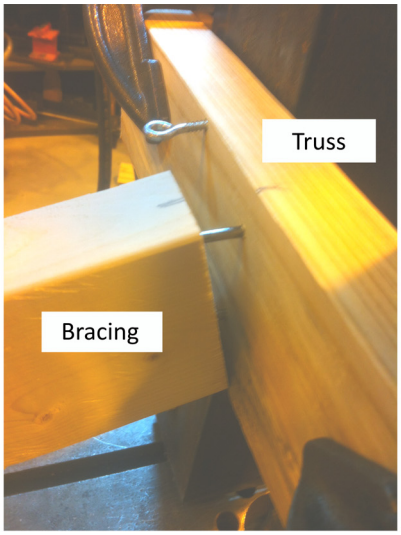

(a)

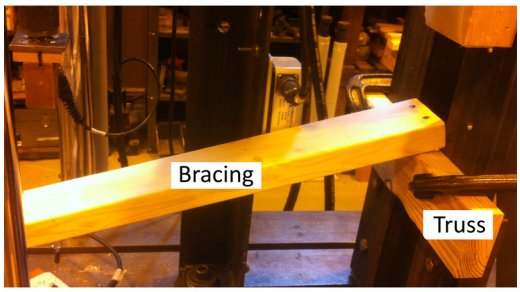

(b)

Fig. 7. Failure mode: (a) discrete bracing; and (b) continuous bracing.

Table 3. Results of truss-to-wall connection rotational stiffness

Test	Average rotational stiffness [N·m/degree (COV)]
10d toenail	21.4 (58.9%)^{E}
SDWC screw	82.0 (31.2%)^{D}
H1Z	317 (18.6%)^{B}
H10A	403 (13.5%)^{A}
HS24	138 (26.1%)^{C}
RT7A tension	158 (11.5%)^{C}
RT7A compression	4.15 (26.5%)^{E}
RT7A both sides	127 (24.6%)^{C,D}
H2.5AZ compression	5.29 (33.5%)^{E}
H2.5AZ both sides	127 (30.5%)^{C}

Note: Superscript letters indicate Tukey's HSD levels of significance.

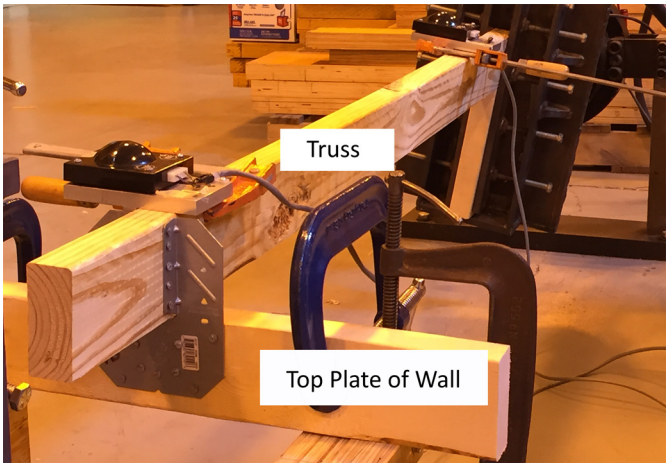

Fig. 8. Rotational stiffness testing of an H10A truss-to-wall connection.

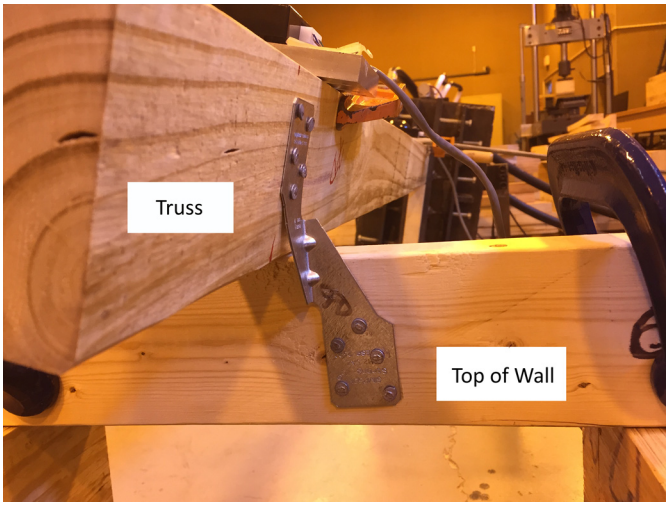

Fig. 9. Rotational stiffness testing of an H2.5AZ compression truss-to-wall connection.

HS24, which has a saddle for both the truss chord and the top plate connections (Fig. 5).

Hurricane ties were proprietary steel plates with a twisted center section so that the two faces of the tie are at 90-degree angles. These connectors included a Simpson Strong-Tie H2.5AZ and a MiTek (Minneapolis, Minnesota) RT7A (Fig. 5). Because of the twist in the hurricane tie, there are both right-handed and left-handed versions.

The twist of the ties caused differences in the direction of load application upon the hurricane ties. A set of the RT7A hurricane ties was tested in both tension, defined as the torque force acting to stretch the hurricane tie, and compression, defined as the torque force acting to compress the hurricane tie. The RT7A connectors were also tested in a double arrangement with two hurricanes per truss chord, resulting in one hurricane tie in tension and one in compression. The H2.5AZ ties were tested in compression and in the double arrangement.

The details of the different truss–wall connections, as well as the number of specimens tested, are given in Table 1. The RT7A tension and compression had 10 specimens and were used for modeling the truss structure previously tested by Morris and Hindman (2017). All other truss–wall connections used eight specimens.

An MTS torsion actuator with a maximum capacity of 5.7 kN·m (50,000 in-lb) and a sensitivity of 5.7 N·m (500 in-lb) applied a rotation of 2°/min to the free end of the 1.83-m (6-ft) truss chord element, as presented in Fig. 6. Testing concluded when the specimen failed or the rotation of the free end reached 30°. The rotation was measured with an Accustar (Ward Hill, Massachusetts) II/DAS20 dual-axis clinometer with an accuracy of $20 \pm 0.01°$. The moment and rotation angle were continuously measured throughout the test, and the graph of the moment M versus rotation θ was used to calculate the slope for the rotational stiffness value [Eq. (1)]. The slope determination was made based on the R^2 values associated with the linear portion of the moment–rotation curve.

Results and Discussion

Discrete and Continuous Bracing Results

The average and coefficient of variation of the rotational stiffness k and the values of the discrete and continuous bracing are shown

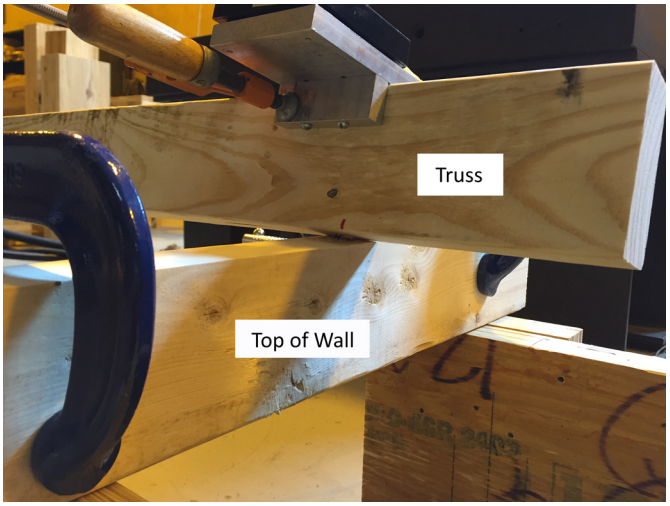

Fig. 11. Rotational stiffness testing of a 10d toenail truss-to-wall connection.

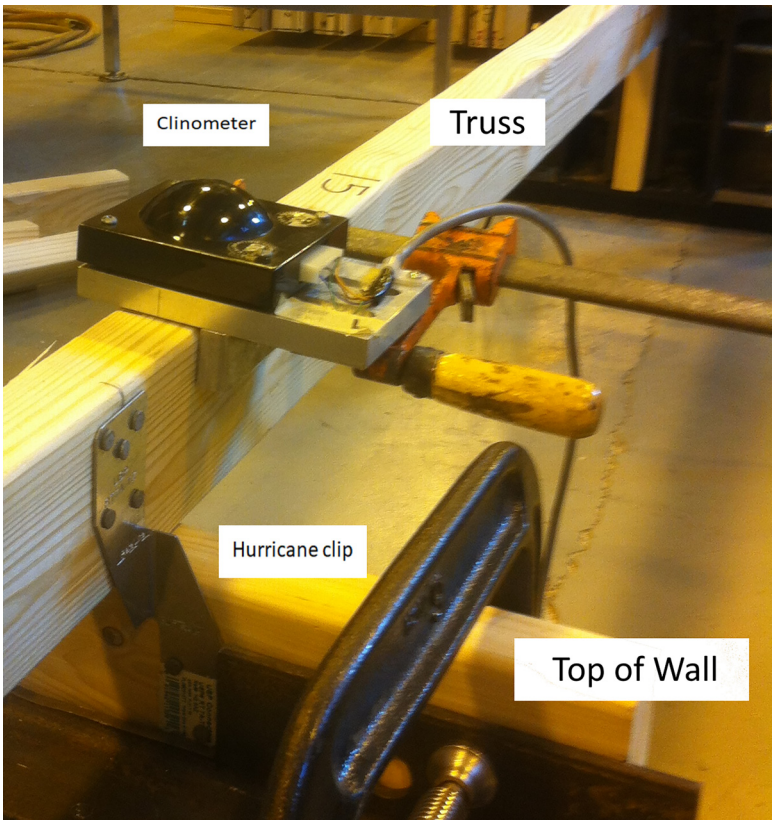

Fig. 10. Rotational stiffness testing of an RT7A tension truss-to-wall connection.

in Table 2. The average discrete bracing rotational stiffness was approximately 4.2 times the average continuous bracing rotational stiffness. The coefficient of variation for the discrete bracing was less than the continuous bracing as well.

Figs. 7(a and b) present the discrete and continuous bracing tests, respectively, after the testing was completed. Rotation of both joints was associated with the withdrawal of the nails, either from the bracing element (discrete bracing) or the truss chord (continuous bracing). In the discrete bracing, the bottom edge of the truss chord acted as a pivot point for the rotation of the bracing element. For the continuous bracing, the bracing element rotated about the front edge of the truss chord.

The rotational stiffness of the discrete and continuous bracing was related to the moment resistance of the fasteners rather than withdrawal properties. It should be noted that the withdrawal strength of the discrete bracing is negligible because the nail was applied to end grain, whereas the withdrawal strength of the continuous bracing can be computed based on the specific gravity of the SP (0.55) truss member (AWC 2015). For the discrete bracing, as presented in Fig. 7(a), the force on the brace pushed the brace downward so that the fastener experienced a combined loading of shear/withdrawal. The pivoting of the brace against the bottom edge of the truss also attempted to deform the nails into a curve, which the nails resisted. For the continuous bracing, the pivoting of the bracing against the face of the truss element caused a prying motion, similar to a crowbar, which loaded the nails almost exclusively in withdrawal. The combined loading of the shear/withdrawal experienced by the discrete bracing likely accounts for the increase in rotational stiffness values.

Truss–Wall Connection Results

The average rotational stiffness values and coefficients of variation for truss–wall connections are given in Table 3. An ANOVA with $\alpha = 0.05$ and a Tukey's honestly significant difference (HSD) test were performed. Considering the type of truss–wall connections as levels, a p-value of 0.001 was found, indicating a significant difference in the rotational stiffness values of the truss–wall connections. The superscript letters in Table 3 indicate levels of significance from the Tukey's HSD test.

The greatest average rotational stiffness value from the truss–wall connections was for the H10A, which was significantly greater than that for all other truss–wall connections. In descending order, the H1Z was significantly different, and then the HS24, RT7A tension, RT7A both sides, and H2.5AZ both sides were not significantly different. Next, the RT7A both sides and the SDWC screw were not significantly different, and finally, the 10d toenail, RT7A compression, and H2.5AZ compression were not significantly different. Lower coefficient of variation (COV) values were associated with the H10A, H1Z, and RT7A tension (11.5–18.6%), whereas greater COV values were associated with the 10d toenail and hurricane tie compression values (26.5–58.9%).

Fig. 8 presents an H10A truss–wall connection near the end of testing. Note that although the wood section had twisted, there was

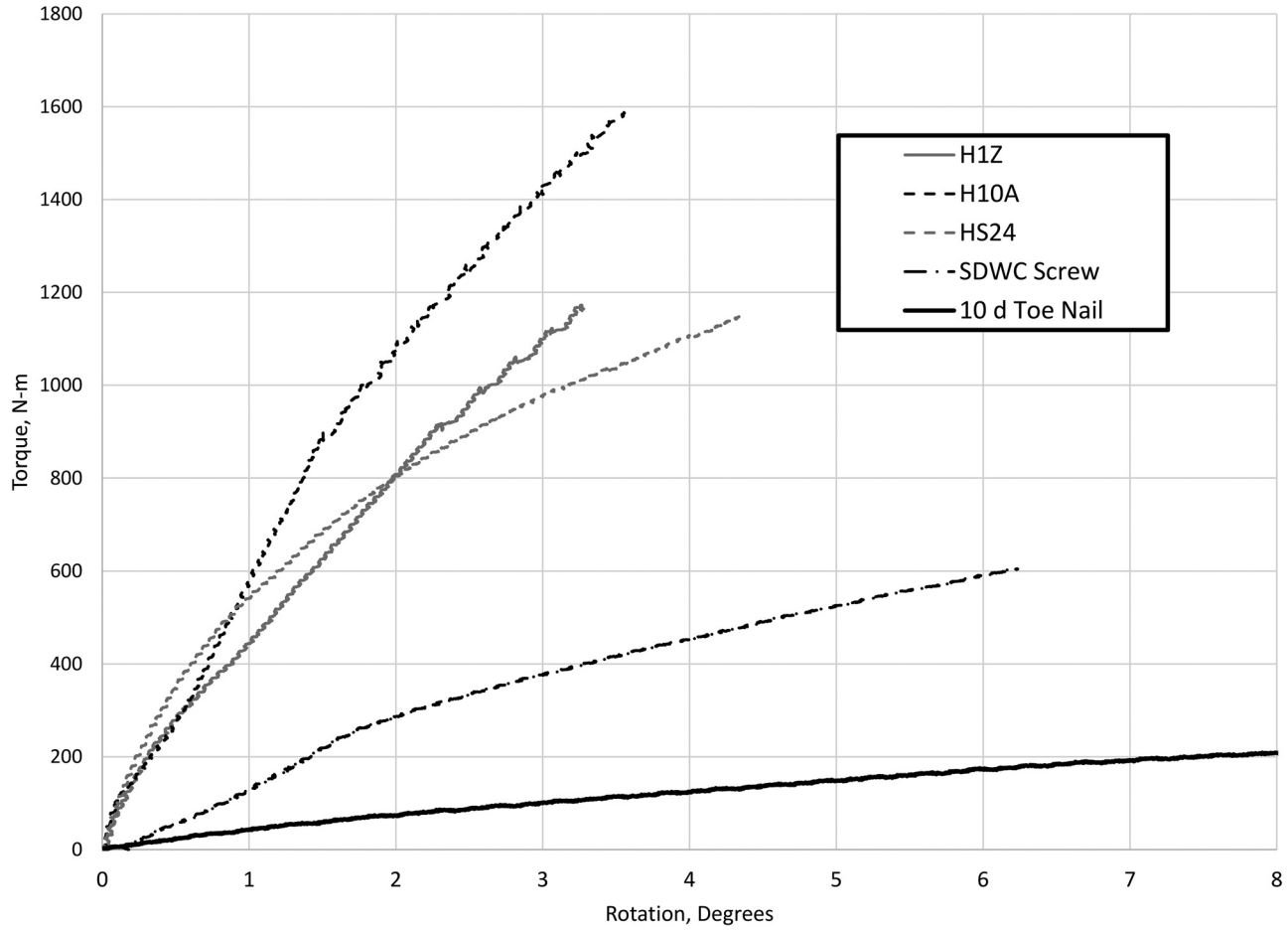

Fig. 12. Moment–rotation graphs of the single-fastener and joist hanger–style truss-to-wall connections.

little deformation within the truss–wall connection itself. This behavior was similar to that of the H1Z truss–wall connections. The compliance of the 2 × 4 truss chord member was greater than the compliance of the truss–wall connection, resulting in less rotation at the truss–wall connection. Fig. 8 also includes the clinometer used for angle measurement (black box and half dome), which was conducted adjacent to the truss–wall connection.

Fig. 9 presents the H2.5AZ compression truss–wall connection after rotational stiffness testing was completed. The hurricane tie was loaded in compression (clockwise rotation in Fig. 9), which acted to fold the hurricane tie. The hurricane ties experienced bending of the sheet metal, noted by the lifting of the hurricane tie off the truss top chord surface at the bottom. Also, the rotation of the truss top chord acted to roll the truss top chord away from the connection because no restraint of movement was present on the other side of the connection.

Fig. 10 presents an RT7A tension truss–wall connection. The torque was applied in a clockwise rotation to the truss chord, acting to stretch the hurricane tie. The hurricane tie was stretched in tension, with shear forces applied to the nails attached. The doubled hurricane ties (RT7A double and H2.5AZ double) also acted similarly to the connection presented in Fig. 9 because one hurricane tie was loaded in tension and the other in compression. The doubled hurricane ties did not experience the shifting of the truss top chord as presented in Fig. 10 due to the presence of the tension hurricane tie on the opposite side. The rotational stiffness values for the doubled hurricane tie were not significantly different from the RT7A tension values due to the RT7A tension rotational stiffness being 38 times the RT7A compression rotational stiffness.

Fig. 11 presents a 10d toenail truss–wall connection near the end of testing. As the torque was applied to the truss top chord, the nail became bent, pulling the truss top chord away from the wall connection. Similar behavior of the SDWC screw was observed when the connection reached the maximum displacement.

Representative moment–rotation curves of the truss–wall connections using joist hangers and single fasteners are presented in Fig. 12. The representative curves are actual moment–rotation curves of specimens with slope values similar to the average value from Table 3. The moment–rotation curves for the H10A, H1Z, and HS24 connections had similar initial slope values. The HS24 connection had a curvilinear behavior, possibly due to the deflection of the double-saddle shape. For the H10A and H1Z curves, the initial smooth curve was followed by a small reduction in slope near 1.5°. The SDWC screw had a higher initial slope until approximately 1.5°, where the slope decreased. This change in slope may represent the bending of the fastener after an initial period of uniform movement of the connection. The 10d toenail had the lowest rotation stiffness of this group and had a linear performance throughout the range of motion. This connection appeared to have started bending as soon as the torsion test began. The joist hanger connections clearly had a greater initial stiffness and continued to maintain higher moment resistance over the range of motion.

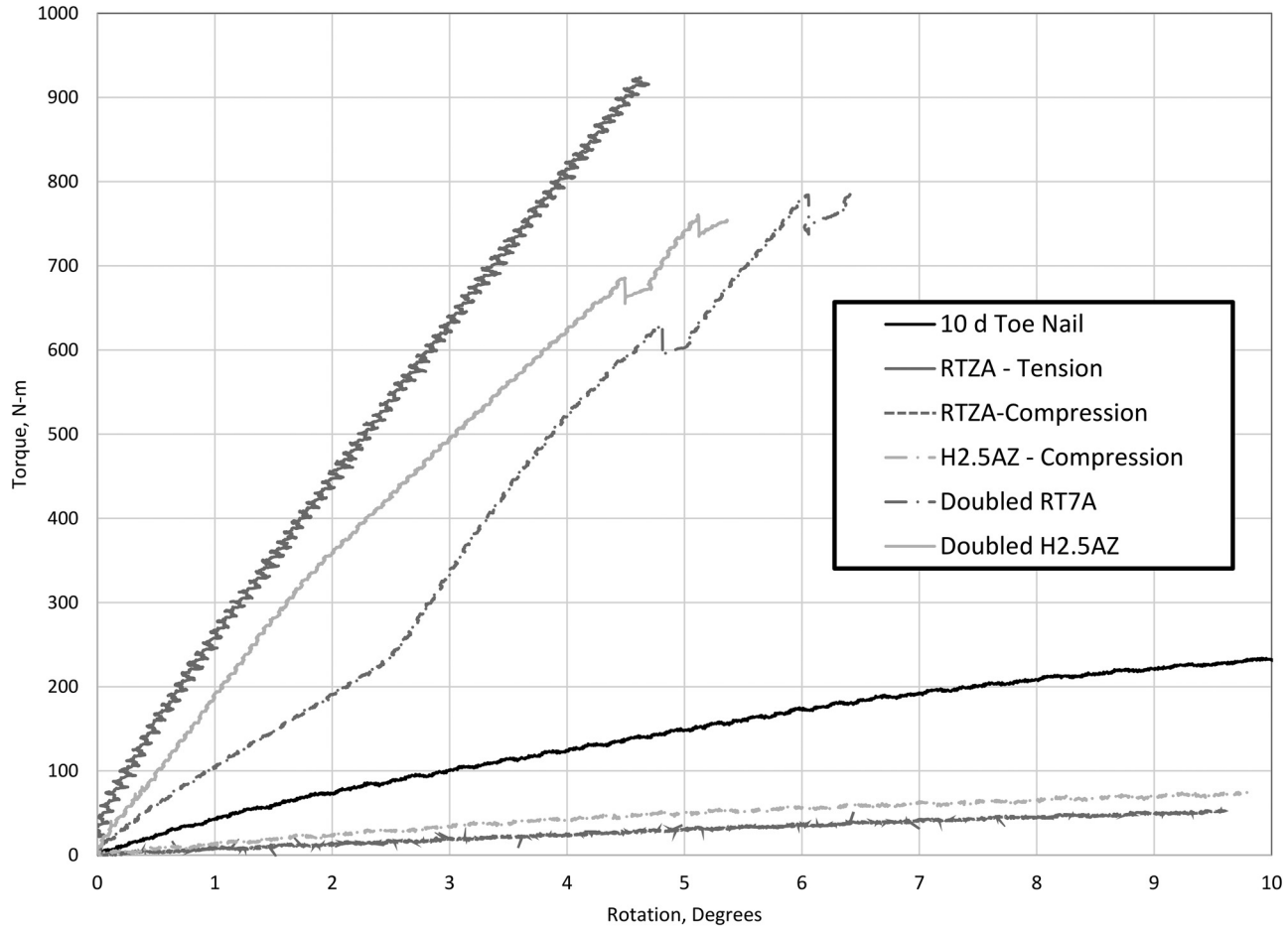

Fig. 13. Moment–rotation graphs of the truss-to-wall connections using hurricane ties.

Representative moment–rotation curves of the truss–wall connections using hurricane ties are presented in Fig. 13. The RT7A tension, RT7A both sides, and H2.5AZ both sides were all much greater than the 10d toenail, the RT7A compression, and the H2.5AZ compression. The curve with the greatest slope in Fig. 13 is that for the RT7A tension, which showed a constant slope throughout the range tested. The RT7A both sides and H2.5AZ both sides performed surprisingly similarly, with both curves demonstrating similar slopes and similar shapes. Also, the RT7A compression and H2.5AZ compression performed similarly. Because of the overall shape and construction of the hurricane ties, the performance between the two manufacturers did not show a difference in the rotational stiffness tested in this study.

The comparisons of the rotational stiffness made previously demonstrate changes in performance between the truss–wall connections using joist hangers, hurricane ties, and single fasteners in rotational loading. At the current time, there is no standardized test method for this analysis, and values of rotational stiffness are not reported by manufacturers. Readers are cautioned in judging the efficacy of particular truss–wall connections based solely on this testing. Further analysis of the effect of rotational stiffness values in MPCWT assembly modeling is needed. Also, truss–wall connections should be judged on a variety of other parameters more commonly applied in buildings, such as resistance to uplift forces and horizontal forces in plane or out of plane with the MPCWT.

Conclusions

The rotational stiffness of MPCWT connections to bracing and walls was measured to provide modeling data for the structural analysis of horizontally applied loads. Bracing methods included discrete, between the chords of the truss, and continuous, over top of the truss. The rotational stiffness of the discrete bracing was greater than that of the continuous bracing.

Truss–wall connections included single fasteners, joist hanger–style connections, and hurricane ties from two different manufacturers. For the truss–wall connections, the joist hanger–style connections had the greatest rotational stiffness, followed by the hurricane ties loaded in tension or doubled, then the single-fastener connections and, finally, the hurricane ties loaded in compression. The hurricane ties loaded in compression experienced bending of the metal cross section and differential movement of the wood members, whereas the tension and double-sided hurricane ties distributed the forces without compromising the tie. No difference in the use of hurricane ties from different manufacturers was found from this testing. Although significant differences in the rotational stiffness of the various connections were found, an investigation of the implications of these differences for the performance of MPCWT assemblies is needed.

Acknowledgments

This work was supported by an award (5R01OH009656) from the National Institute for Occupational Safety and Health (NIOSH) of the Centers for Disease Control and Prevention (CDC). Its contents are solely the responsibility of the authors and do not necessarily represent the official views of the CDC. This work was also supported by the National Institute of Food and Agriculture of the US Department of Agriculture (USDA), McIntire Stennis Project 0229938.

References

AISI (American Iron and Steel Institute). 2001. *Commentary on the standard for cold-formed steel framing—Truss design*. Washington, DC: AISI, Committee on Framing Standards (COFS).

AWC (American Wood Council). 2015. *National design specification for wood construction (NDS)*. Leesburg, VA: AWC.

DeRenzis, A., V. Kochkin, and X. Wang. 2012. *Evaluation of the lateral performance of roof truss-to-wall connections in light-frame wood systems*. Rep. No. FPL-GTR-214. Madison, WI: Forest Products Laboratory.

Gupta, R., K. G. Gebremedhin, and J. R. Cooke. 1992. "Analysis of metal-plate-connected wood trusses with semi-rigid joints." *Trans. Am. Soc. Agric. Eng.* 35 (3): 1011–1018. https://doi.org/10.13031/2013.28695.

Kanerva P., S. Peltola, and J. Vesa. 2004. "Design methods for utilization of rotational stiffness of mechanical joints on the design of timber structures." In *Proc., 8th World Conf. of Timber Engineering*. Helsinki, Finland: Finnish Association of Civil Engineers.

Kassimali, A. 2010. *Structural analysis*. 4th ed. Boston: Cengage Learning.

Koch, L. M., D. P. Hindman, and T. Smith-Jackson. 2016. "Metal plate connected wood trusses exposed to out of plane lateral loads." *J. Archit. Eng.* 22 (3): B4016001. https://doi.org/10.1061/(ASCE)AE.1943-5568.0000203.

Morris, J. C., and D. P. Hindman. 2017. "Effect of bracing and anchor choice on the strength of metal plate-connected wood-truss assemblies carrying fall-arrest loads." *J. Archit. Eng.* 23 (3): B4017001. https://doi.org/10.1061/(ASCE)AE.1943-5568.0000247.

Šilih, S., S. Kravanja, and M. Premrov. 2010. "Shape and discrete sizing optimization of timber trusses by considering of joint flexibility." *Adv. Eng. Software* 41 (2): 286–294. https://doi.org/10.1016/j.advengsoft.2009.07.002.

Šilih, S., M. Premrov, and S. Kravanja. 2005. "Optimum design of plane timber trusses considering joint flexibility." *Eng. Struct.* 27 (1): 145–154. https://doi.org/10.1016/j.engstruct.2004.10.001.

Zaharia, R., and D. Dubina. 2006. "Stiffness of joints in bolted connected cold-formed steel trusses." *J. Constr. Steel Res.* 62 (3): 240–249. https://doi.org/10.1016/j.jcsr.2005.07.002.